scientific reports

Check for updates

OPEN

Rhomboid-like 2 correlated with TME infiltration inhibits cuproptosis-related genes and drives malignant phenotype in clear cell renal cell carcinoma

Zhifei Che[1,4], Wenyi Jin[2,4], Yaoxi Wu[1], Haoyong Li[3]✉ & Peiyu Liang[1]✉

The crosstalk between cuproptosis and the tumor immune microenvironment (TIME) is vital during clear cell renal cell carcinoma (ccRCC) malignant progression. However, the underlying molecular mechanisms regulate this cross-talk remain elusive. Through tailored machine learning, we analyze clinical ccRCC data from The Cancer Genome Atlas (TCGA) to explore the critical factors that regulate the interaction among cuproptosis, TIME, and tumor progression. We found that rhomboid-like 2 (RHBDL2), critical gene affecting this process, might inhibit cuproptosis-related genes (CRGs) and promotes ccRCC progression through the Wnt/β-catenin pathway. Next, knocking down RHBDL2 expression increased the cuproptosis-related genes ferredoxin 1 (FDX1) and lipoic acid synthase (LIAS) levels but reduced forkhead box P3 (FOXP3) levels and tumor growth in vivo and in vitro models. By employing HLY78, Wnt/β-catenin pathway activator, we rescued the expression of CRGs and the malignant proliferation and metastasis capacity in ccRCC cells with RHBDL2 knockdown. Mechanistically, RHBDL2 inhibits cuproptosis and promotes malignant progression of ccRCC through the Wnt/β-catenin pathway. Abnormal RHBDL2 expression may cause the suppressive TIME formation by regulating Treg-cell infiltration, thus triggering immune escape. In summary, our results indicated that RHBDL2 is an oncogene that induces tumorigenesis and targeting RHBDL2 may be novel therapeutic direction for metastatic ccRCC.

Keywords Rhomboid-like 2, Cuproptosis, Wnt/β-catenin, Regulatory T cells, Clear cell renal cell carcinoma

Abbreviations

ccRCC	Clear cell renal cell carcinoma
TIME	Tumor immune microenvironment
TME	Tumor microenvironment
RHBDL2	Rhomboid-like 2
CRGs	Cuproptosis-related genes
Treg	Regulatory T
FOXP3	Forkhead box
FDX1	Ferredoxin 1
LIAS	Lipoic acid synthase
TIICs	Tumor-infiltrating immune cells

Clear cell renal cell carcinoma (ccRCC) accounts for about 75% of all cases of renal cancer. Originating in the epithelial cells of the renal proximal convoluted tubule, ccRCCs are highly malignant and tend to metastasize at advanced stages, resulting in a poor prognosis[1,2]. In recent years, ccRCC incidence has increased rapidly

[1]Department of Urology, The First Affiliated Hospital of Hainan Medical University, No. 31 Longhua Road, Longhua District, Haikou 570102, Hainan Province, China. [2]Department of Biomedical Sciences, College of Veterinary Medicine and Life Sciences, City University of Hong Kong, Kowloon Tong 999077, Hong Kong SAR, China. [3]Department of Urology, Renmin Hospital of Wuhan University, No. 99 Zhang Road, Wuchang District, Wuhan 430060, Hubei Province, China. [4]Zhifei Che and Wenyi Jin contributed equally to this work. ✉email: RM002243@whu.edu.cn; PeiyuLiangUrinary@163.com

worldwide; approximately 75,000 new ccRCC cases and 14,000 ccRCC-related deaths were reported in 2022[3]. Despite continuous progress in the development of targeted drug therapy and robotic surgery, as well as the rise of immunotherapy, patients with ccRCC encounter several issues, including poor drug efficacy and off-target and drug resistance; nearly one-third of the patients still demonstrate local recurrence or distant metastasis during treatment at advanced stages[4,5]. Hence, developing new molecular targets and therapeutic methods for ccRCC, as well as defining the regulatory mechanism linked to the malignant advancement of ccRCC, is imperative for newer therapeutic strategy design and development and ccRCC-related mortality reduction.

Copper, an essential micronutrient, is widely involved in the physiological and biochemical processes of various cell types in the human body[6]. In 2022, Tsvetkov et al. first reported cuproptosis, a unique mode of cell death regulated by excessive copper[7]. Cuproptosis, initiated by Cu^{2+}bound directly to lipoylated mitochondrial enzymes during the tricarboxylic acid cycle, leads to abnormal protein aggregation, proteotoxic stress, and eventual cell death[8]. Notably, an imbalance in copper homeostasis contributes to the emergence and progression of various illnesses and cancers[9,10]. Cuproptosis-related genes (CRGs), including ferredoxin 1 (*FDX1*), lipoic acid synthase (*LIAS*), dihydrolipoamide S-acetyltransferase (*DLAT*), pyruvate dehydrogenase E1 subunit beta (*PDHB*), ATP7A and ATP7B, have crucial roles in cuproptosis, as well as the regulatory cuproptosis pathway[6,7]. Several studies have postulated that changes in CRGs are promising biomarkers for predicting prognosis and evaluating immunotherapeutic responses in various cancers, including ccRCC[11–13]. Dysregulated cuproptosis leads to an abnormal tumor microenvironment (TME) and molecular characteristics, resulting in adverse prognoses of cancers, such as hepatocellular carcinoma and breast cancer. However, the specific molecular regulatory mechanisms underlying cuproptosis in ccRCC remain unclear, and a dearth of effective experimental validation of these mechanisms limits the clinical translational of cuproptosis for ccRCC treatment.

Human rhomboid-like 2 (RHBDL2), located on the eukaryotic plasma membrane, is a member of the rhomboid protein family of intramembrane protease. It is composed of serine proteases and their homologs, which contain seven transmembrane domains[14]. RHBDL2 enacts its function through serine proteases. These serine proteases use active sites within the lipid bilayer to hydrolyze substrate transmembrane domains, silencing or activating integral proteins' functions[15,16]. RHBDL2 cleaves substrate EGF ligand[14]and NOTCH receptor[17], activating the protooncogenes *EGFR*[18] and *NOTCH*[19], respectively, and thus induces carcinogenesis. In other words, RHBDL2, a serine proteolytic enzyme, may promote tumorigenesis by activating protooncogenes or eliminating tumor suppressor genes through hydrolysis. Chen et al. reported that pancreatic cancer tissue demonstrates a high expression of RHBDL2; its serine proteases cleave NOTCH1, activating the NOTCH pathway and thus accelerating pancreatic cancer cell proliferation, migration, and invasion both in vitro and in vivo[17]. However, the regulatory mechanism of RHBDL2, its effect on tumor progression, and its clinical implications in ccRCC remain unclear. In addition, studies on the influence of RHBDL2 on cuproptosis and the related regulatory mechanisms are lacking.

Adaptive and innate immune cells infiltrate and alter the TME, forming a microecosystem that regulates various aspects of tumor development and immunotherapy response[20]. Some recent studies have comprehensively analyzed the immune landscape of the TME and suggested a correlation between cuproptosis and the tumor immune microenvironment (TIME) in hepatocellular carcinoma[21]. However, the specific functions of RHBDL2 and cuproptosis in various TIME cells during ccRCC progression remain unclear.

In this study, we used RNA-sequencing (RNA-seq) data from The Cancer Genome Atlas (TCGA) combined with multiple bioinformatics algorithms to identify *RHBDL2* as a pivotal gene associated with CRGs. In addition, TCGA RNA-seq data have been obtained from both tumor and normal samples; therefore, to increase the accuracy of our analysis, we deconvoluted these data to focus on gene expression in tumor samples. Our results revealed that abnormal *RHBDL2* expression is related to a critical signaling pathway and immune cell infiltration levels in ccRCC TME. Next, we analyzed *RHBDL2*, *FDX1*, *LIAS*, and forkhead box P3 (*FOXP3*) expression levels in ccRCC tissues and the corresponding paracancerous (PC) tissues to evaluate the relationship between RHBDL2, CRGs, and regulatory T (Treg)-cell infiltration levels. We constructed in vitro and in vivo *RHBDL2*-knockdown models to analyze the effects of RHBDL2 on *FDX1*, *LIAS*, and *FOXP3* expression in ccRCC cells, as well as their metastasis and proliferation. Furthermore, by activating the Wnt/β-catenin pathway, we restored CRG expression and the malignant phenotype. Taken together, our results indicated that *RHBDL2* is a new potential therapeutic target associated with both cuproptosis and the TIME in ccRCC.

Result

Effects of cuproptosis on clinical characteristics and survival of patients with ccRCC

Our results indicated that the expression of CRGs was significantly lower in the ccRCC tumor tissue than in the normal kidney tissue (Fig. 1A). This suggests that cuproptosis plays a pivotal role in ccRCC development. Consequently, we used a cutoff value of 0.006797 to classify patients with ccRCC into high- and low-cuproptosis groups (Fig. 1B and C). Patients exhibiting high cuproptosis levels demonstrated better overall survival (OS) than those with low cuproptosis levels (Fig. 1D). In other words, increased cuproptosis activity might indicate a favorable ccRCC prognosis. Moreover, cuproptosis activity was significantly diminished in patients with advanced ccRCC including a high pathological grade (Fig. 1E), tumor (T) stage (Fig. 1F), and metastasis (M) stage (Fig. 1H); however, no cuproptosis activity changes were noted in relation to the node (N) stage (Fig. 1G). Therefore, a decrease in cuproptosis activity may enhance ccRCC progression and metastasis.

RHBDL2: a pivotal gene linked to cuproptosis regulation and ccRCC progression

Using univariate Cox regression and the KM survival curve, we identified 2,182 genes associated with the cuproptosis pathway and ccRCC progression. Based on our prior findings, we established these criteria for screening key genes associated with ccRCC development according to reduced cuproptosis activity: (i) hazard ratio (HR) > 1 and Cox $P < 0.001$; (ii) KM $P < 0.001$; (iii) Spearman correlation coefficient for cuproptosis

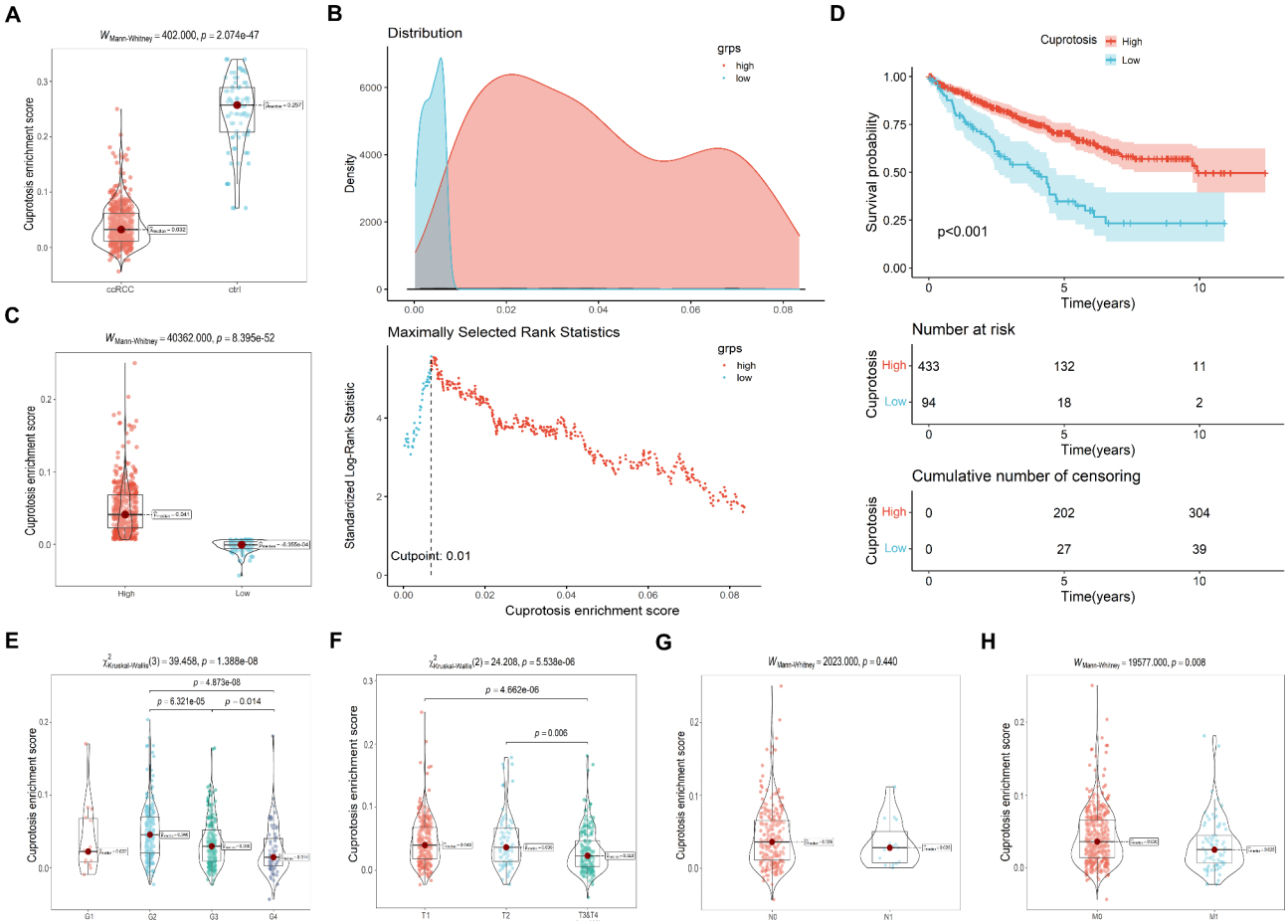

Fig. 1. Clinicopathological significance of cuproptosis in ccRCC. (A) A violin plot showing a significant difference in cuproptosis activity between ccRCC and normal samples; it is composed of a box plot, a kernel density plot, medians, and each data point of cuproptosis activity. (B) Classification of 527 patients with ccRCC into high- and low-cuproptosis groups according to the cutoff value. (C) Cuproptosis activity of ccRCC cells compared between the high- and low-cuproptosis groups. (D) KM survival curves for survival probability of high- and low-cuproptosis patients with ccRCC. (E–H) Correlation analysis between cuproptosis and clinical parameters in ccRCC patients: pathological grade (E), tumor stage (F), node stage (G), and metastasis stage (H).

activity < 0. Of the 2,182 genes, the top 20 key genes were confirmed (Fig. 2A and B). Finally, because of its higher HR and lower Spearman coefficient values, *RHBDL2* was finally identified as the main gene underlying the relationship of the cuproptosis pathway with ccRCC development. In particular, an inverse relationship was noted between *RHBDL2* expression and the key cuproptosis markers *FDX1* and *LIAS*[7], bolstering the cuproptosis pathway in ccRCC (Fig. 2C and E).

Furthermore, the ccRCC samples demonstrated elevated *RHBDL2* expression compared with the normal samples (Fig. 3A and B). By using a cutoff value of 0.598817, we categorized the clinical patients into high- and low-RHBDL2 groups to explore the *RHBDL2* expression–survival relationship (Fig. 3C). As shown in Fig. 3D, clinical patients with higher *RHBDL2* expression experienced shorter OS than their lower *RHBDL2* expression counterparts. *RHBDL2* expression was higher in patients with advanced ccRCC, specifically in those with an advanced grade (Fig. 3E) and TNM stage (Fig. 3F and H). To further validate the precision of the effects of RHBDL2 on clinical survival, a time-dependent receiver operating characteristic (ROC) curve was constructed at 1 year according to the RHBDL2 score, comparable to that of TNM staging and pathological grading and their predictive power (Fig. 3I). Thus, *RHBDL2* might be a potent biomarker for predicting survival prognosis in patients with ccRCC. Taken together, these results clarify the crucial role of RHBDL2 in regulating cuproptosis activity and facilitating distant metastasis and poor survival in patients with ccRCC.

Correlation among *RHBDL2*, cuproptosis pathway, and TIME characteristics

To investigate the relationship between *RHBDL2* expression and tumor immune infiltration, we used the ESTIMATE algorithm and analyzed the distinct TIME statuses between the high- and low-RHBDL2 groups. As presented in Fig. 4A and C, patients with high RHBDL2 expression had considerably higher immune and ESTIMATE scores but considerably lower tumor purity than patients with low RHBDL2 expression. However,

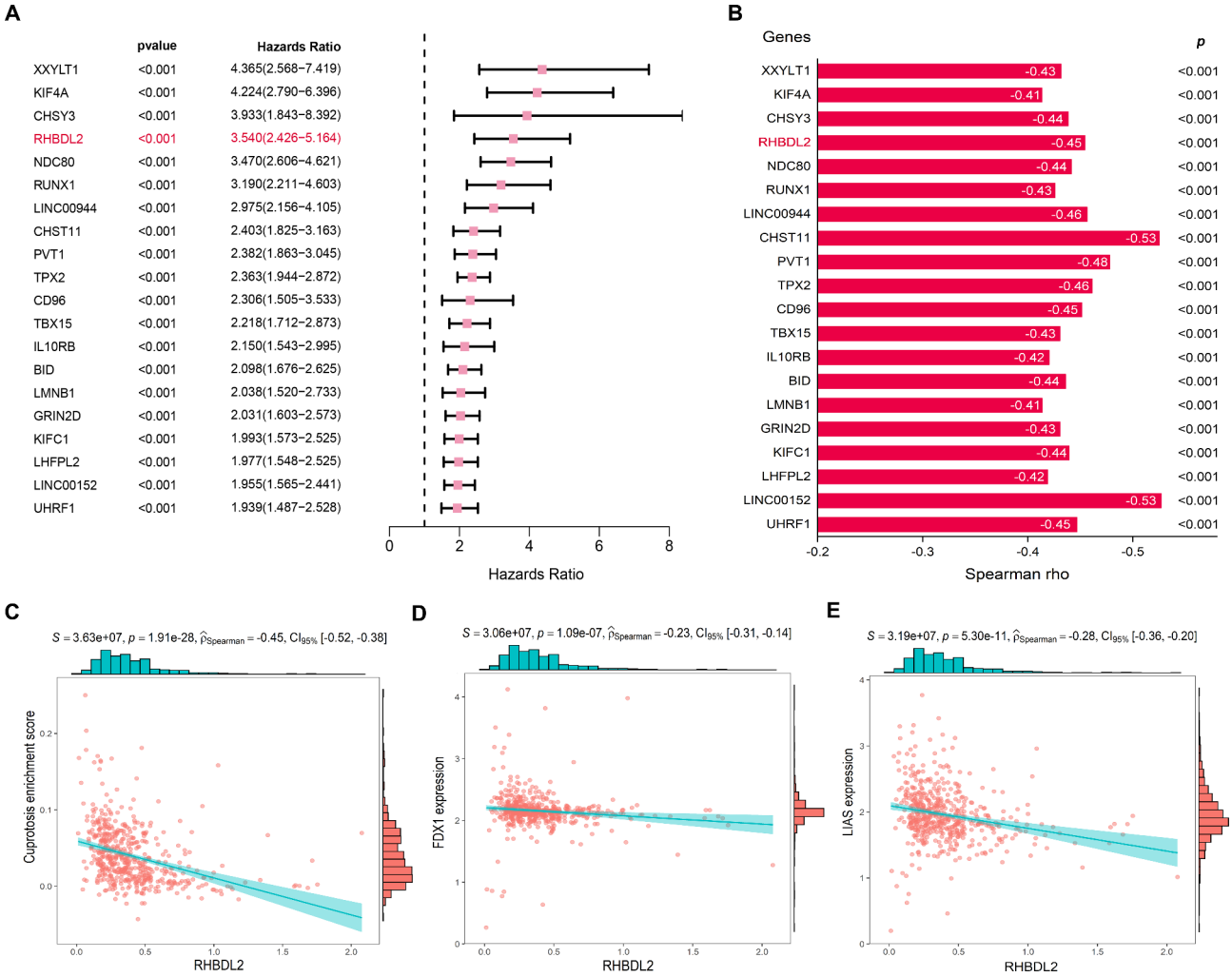

Fig. 2. *RHBDL2*: a key gene associated with the cuproptosis pathway involved in ccRCC development. (A) A forest plot showing the top 20 related genes for *P* values and HRs in univariate Cox regression analysis. (B) Spearman correlation coefficient analysis with the cuproptosis activity. (C–E) Correlation of *RHDBL2* expression with cuproptosis activity (C), *FDX1* expression (D), and *LIAS* expression (E) in ccRCC.

no significant difference was noted in the stromal scores between the high- and low-RHBDL2 groups (Fig. 4D). Thus, *RHBDL2* expression may influence immune functionalities in the TME of patients with ccRCC. Therefore, to explore the effect of RHBDL2 on immune infiltration in depth, we used CIBERSORT and ssGSEA algorithms and assessed the relative infiltration intensity and infiltration patterns of 29 distinct immune cell types in the TIME of ccRCC samples, respectively. Our results demonstrated that the infiltration levels of immune cells were relatively high in patients with ccRCC; moreover, the proportion of tumor-infiltrating immune cells (TIICs) considerably increased with an increase in *RHBDL2* expression (Fig. 4E and F). In total, 19 TIICs displayed significant infiltration profile and correlation differences between the high- and low-RHBDL2 groups. Of them, 16 TIICs, including Treg cells, antigen-presenting cells, T cells, and inflammation-promoting cells, were positively correlated with *RHBDL2* expression levels; however, the remaining three TIICs were negatively correlated with *RHBDL2* expression levels (Supplementary Fig. 1A–1 H). This indicates a potential strong association between *RHBDL2* expression and TIICs.

The results also revealed that Treg-cell count was considerably higher in patients with high RHBDL2 expression, and a strong association was discerned between high Treg-cell infiltration and unfavorable outcomes in ccRCC cases, verifying the presence of a suppressive TIME (Supplementary Fig. 1G). We also discovered a positive correlation between RHBDL2 and the biomarker FOXP3 levels in Treg cells in TCGA-ccRCC array[24]. Furthermore, our correlation analysis indicated that Treg-cell infiltration levels were inversely proportional to cuproptosis activity (Supplementary Fig. 2A). The presence of the CRGs *FDX1* and *LIAS*involved in the cuproptosis pathway was inversely proportional to Treg-cell infiltration rates. Our data thus confirmed that cuproptosis is inversely related to RHBDL2 levels (Supplementary Fig. 2B and 2 C). Taken together, these results suggested that RHBDL2 suppresses the cuproptosis pathway, leading to enhanced Treg-cell infiltration[25].

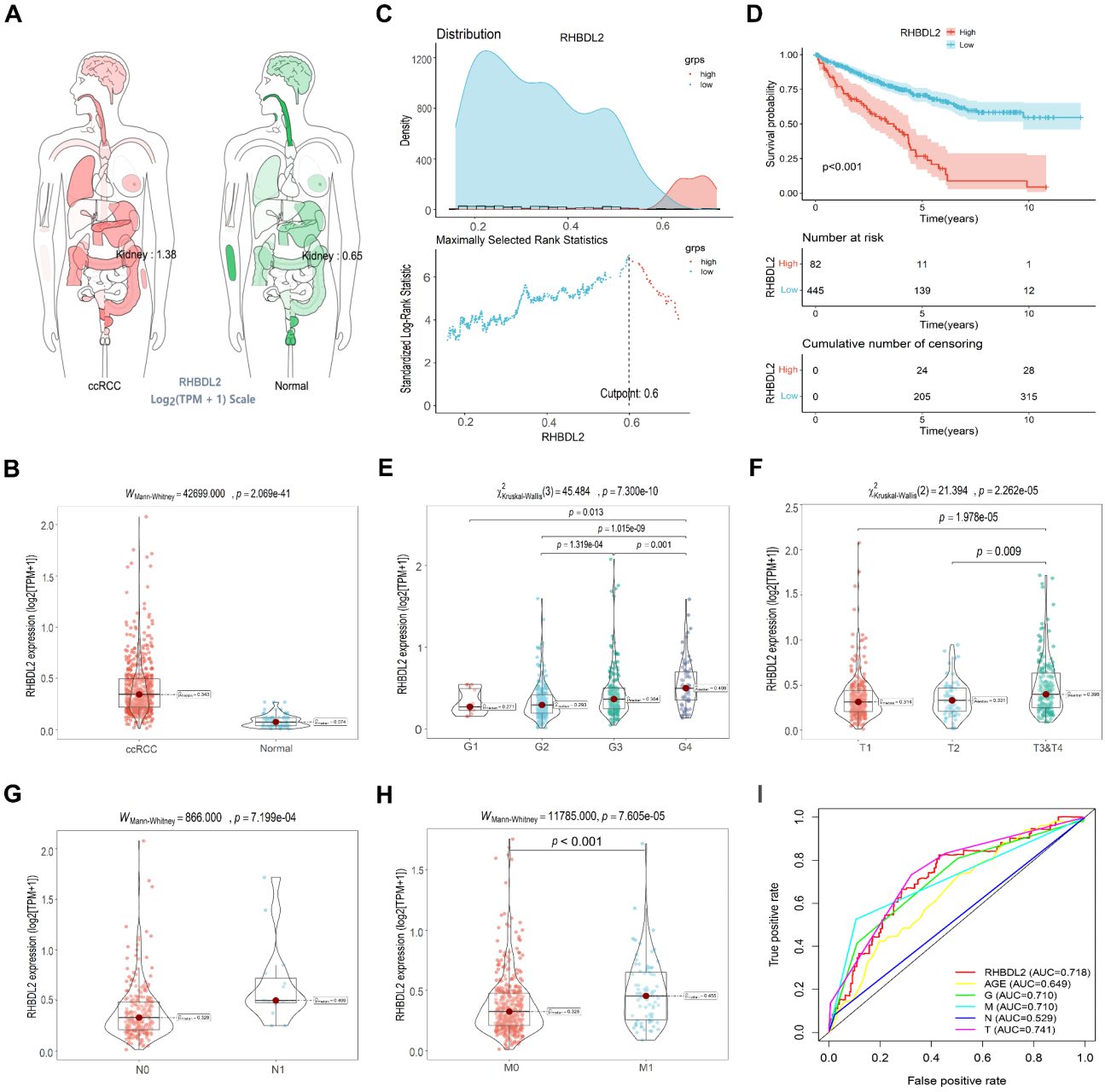

Fig. 3. Clinical implications and survival probability related to RHBDL2 in ccRCC samples. (A, B) Expression levels of *RHBDL2* in ccRCC and normal clinical samples in TCGA databases. (A) An anatomy plot presenting mean RHBDL2 levels (ccRCC: 1.38, Normal: 0.65). (B) A violin plot composed of a box plot, a kernel density plot, and medians of *RHBDL2* levels (ccRCC: 0.343, Normal: 0.074). (C) Classification of the high- and low-RHBDL2 patients with ccRCC according to the cutoff value. (D) Survival probability analysis of the high- and low-RHBDL2 patients with ccRCC. The results demonstrate significant differences in survival probability between the high- and low-RHBDL2 groups. (E–H) Correlation analyses between RHBDL2 expression and clinical parameters including pathological grade (E), tumor stage (F), node stage (G), and metastasis stage (H). (I) ROC curve of *RHBDL2* expression for the sensitivity and specificity of 1-year survival, TNM stage, grade, and age in patients with ccRCC.

Correlation among *RHBDL2*, cuproptosis activity, and Wnt/β-catenin pathway

To further elucidate the regulatory mechanisms and pathways underlying the cuproptosis–*RHBDL2* association, we investigated several critical pathways involved in ccRCC pathogenesis through Spearman correlation analysis (Supplementary Fig. 2D). Our findings indicated a positive association between RHBDL2 expression and the Wnt/β-catenin pathway. The Wnt/β-catenin pathway also showed an inverse relationship with cuproptosis activity (Supplementary Fig. 2E). Thus, these results suggested that RHBDL2 modulates cuproptosis activity through the Wnt/β-catenin pathway. In summary, through machine learning, we preliminarily found that

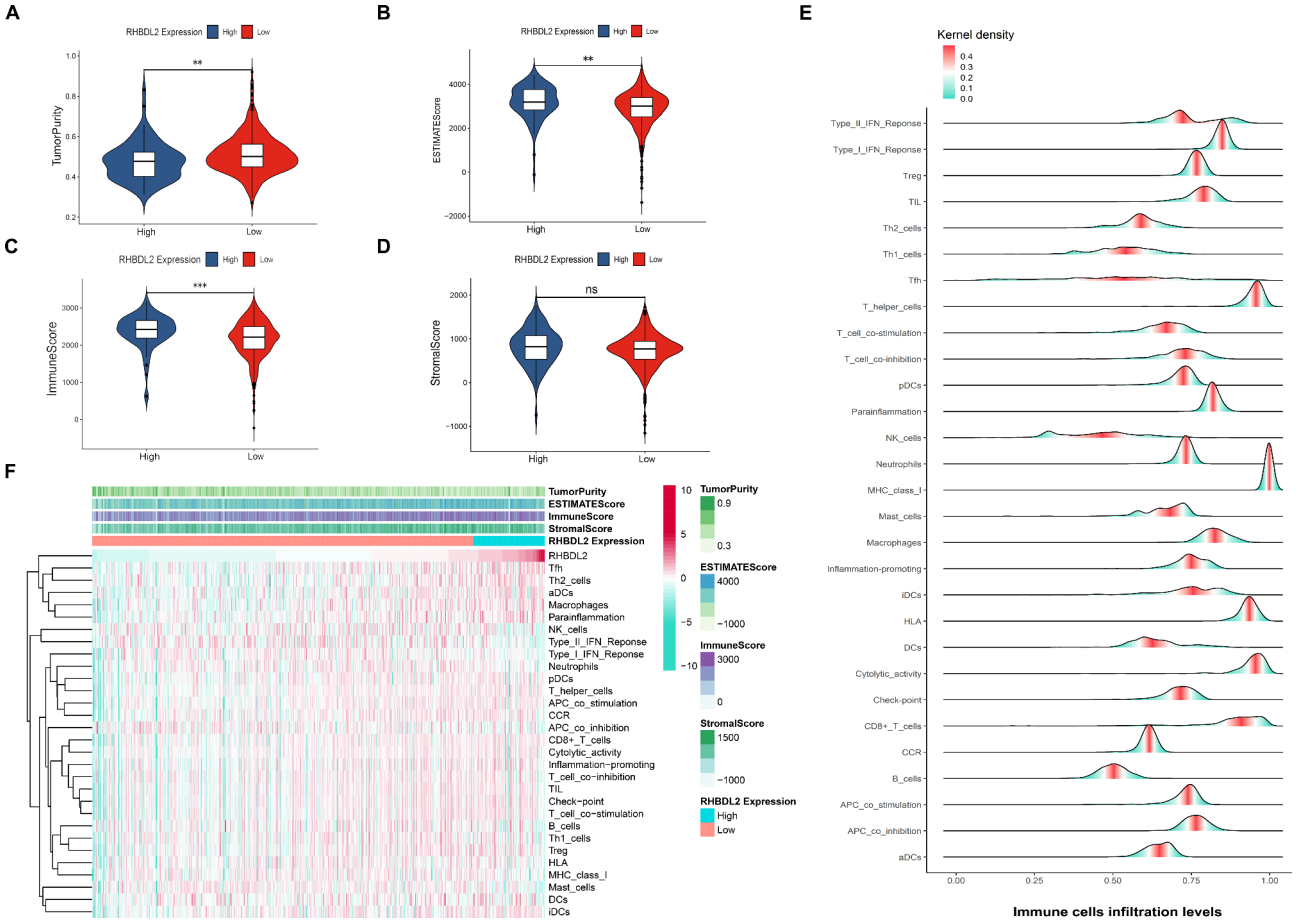

Fig. 4. Machine-learning algorithm analysis for TME of patients with two expression groups to survey immune infiltration. (A) A violin plot of tumor purity in two groups, representing a considerably lower tumor purity in the high-RHBDL2 group than in the low-RHBDL2 group. (B) A violin plot of ESTIMATE score showing a considerably higher score in the high-RHBDL2 group than in the low-RHBDL2 group. (C) A violin plot showing a significantly higher immune score in the high-RHBDL2 group than in the low-RHBDL2 group. (D) A violin plot showing no significant differences in stromal scores between the high- and low-RHBDL2 groups. (E) A kernel density ridgeline plot showing the integral infiltration levels of 29 immune cell types in 527 ccRCC samples. (F) A heatmap of ssGSEA algorithm analyses the infiltration differences in tumor purity, ESTIMATE score, immune score, stromal score, and RHBDL2 level in 29 immune cells between the high- and low-RHBDL2 groups. $^{**}P<0.01$, $^{***}P<0.001$; ns, nonsignificant.

RHBDL2 may inhibit cuproptosis activity via the Wnt/β-catenin pathway and then increase Treg-cell infiltration levels, leading to suppressive TIME formation.

Validation of high *RHBDL2* expression and Treg-cell infiltration and low CRG expression in human ccRCC tissue samples

To verify the accuracy and validity of our bioinformatics prediction results before clinical application, we assessed 12 clinical samples with ccRCC and their matched PC tissues to analyze the expression of RHBDL2, FDX1, LIAS, and FOXP3 (a Treg-cell biomarker) through Western blotting and IHC; this was followed by HE staining to observe the cell morphology and structure. RHBDL2 and FOXP3 expression levels were considerably higher in the tumor tissue than in the PC tissue in both the Western blots (0.77 ± 0.19 vs. 0.29 ± 0.15 and 0.93 ± 0.11 vs. 0.34 ± 0.16, respectively) and the IHC Sect. (59.02 ± 7.56 vs. 13.93 ± 6.14 and 40.62 ± 10.58 vs. 10.29 ± 3.76, respectively). However, the tumor tissue demonstrated substantial attenuation of FDX1 and LIAS expression compared with the PC tissue in both the Western blots (0.47 ± 0.16 vs. 0.75 ± 0.24 and 0.17 ± 0.08 vs. 0.80 ± 0.20, respectively) and the IHC Sect. (32.79 ± 7.66 vs. 75.44 ± 8.53 and 35.55 ± 8.57 vs. 79.11 ± 7.14, respectively; both $P<0.01$; Fig. 5A and D). In addition, the HE results demonstrated that the tumor cells had severely damaged the normal glomerular and renal tubular epithelial structures; moreover, the tumor cells were transparent and disordered relative to the normal renal tissue (Fig. 5C). Through IF staining, we further assessed RHBDL2, FDX1, and FOXP3 expression and colocalization in the tumor and PC tissues (Fig. 5E). Compared with the PC tissue, the tumor tissue had considerably lower FDX1 expression but higher RHBDL2 and FOXP3 expression. This finding confirmed that RHBDL2, FDX1, and FOXP3 expression are closely linked in all ccRCC tissues.

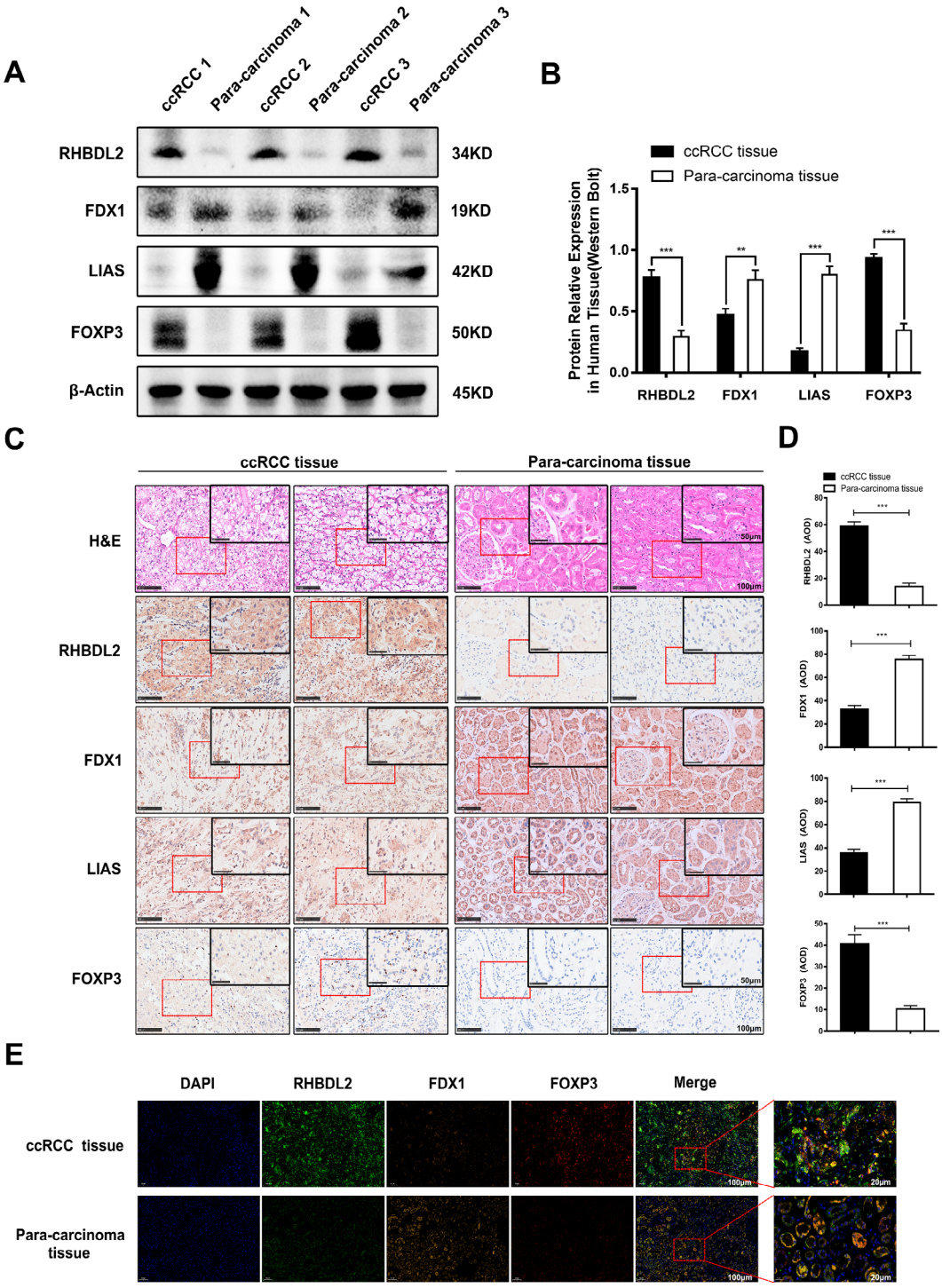

Fig. 5. RHBDL2, FDX1, LIAS, and FOXP3 expression in ccRCC and PC tissues. (A, B) Western blot for relative expression levels of RHBDL2, FDX1, LIAS, and FOXP3 in the ccRCC and PC tissues (original blots are presented in Supplementary Fig. 4). (B) Quantitative analysis of Western blotting results. RHBDL2 and FOXP3 expression levels were significantly higher in the ccRCC tissues than in the PC tissues (0.77 ± 0.19 vs. 0.29 ± 0.15 and 0.93 ± 0.11 vs. 0.34 ± 0.16, respectively). In contrast, FDX1 and LIAS expression levels were lower in the ccRCC tissues than in the PC tissues (0.47 ± 0.16 vs. 0.75 ± 0.24 and 0.17 ± 0.08 vs. 0.80 ± 0.20, respectively). (C, D) Representative images of IHC and HE staining for RHBDL2, FDX1, LIAS, and FOXP3 expression showing structural and morphological changes in ccRCC and PC tissue samples (magnifications: 100× and 200×, scale bars: 100 and 50 μm). (E) IF staining for RHBDL2 (green), FDX1 (yellow), and FOXP3 (red) localization and expression in ccRCC and PC tissue samples (magnifications: 100× and 500×, scale bars: 100 and 20 μm). Nuclei are counterstained using DAPI (blue). All data are expressed as means ± SDs. $^{**}P < 0.01$, $^{***}P < 0.001$.

Consequently, *RHBDL2* might act as an oncogene and participate in the modulation of cuproptosis activity and Treg-cell infiltration in patients with ccRCC.

Validation of *RHBDL2* knockdown inhibiting proliferative, migratory, and invasive abilities of ccRCC cells in vitro model

To explore the impact of RHBDL2 on the malignant phenotype of ccRCC cells in vitro, we first knocked down *RHBDL2* expression specifically in 769-P and 786-O cells by using siRNAs against *RHBDL2* (siRNA-1, siRNA-2, and siRNA-3). For negative control, the cells were transfected with si-Ctrl. According to our Western blotting results, 769-P and 786-O cells demonstrated a significant attenuation in RHBDL2 expression after transfection with siRNA-1 (0.25 ± 0.04 and 0.42 ± 0.10, respectively) compared with that after transfection with blank (0.47 ± 0.07 and 0.82 ± 0.12, respectively), si-Ctrl (0.56 ± 0.09 and 0.87 ± 0.16, respectively), siRNA-2 (0.31 ± 0.10 and 0.73 ± 0.14, respectively), or siRNA-3 (0.37 ± 0.03 and 0.76 ± 0.11, respectively; all $P < 0.05$; Fig. 6A and B). The CCK-8 assay further revealed that 769-P and 786-O cell proliferation was considerably attenuated after *RHBDL2*-knockdown using siRNA-1 compared with that after *RHBDL2*-knockdown using si-Ctrl, siRNA-2, or

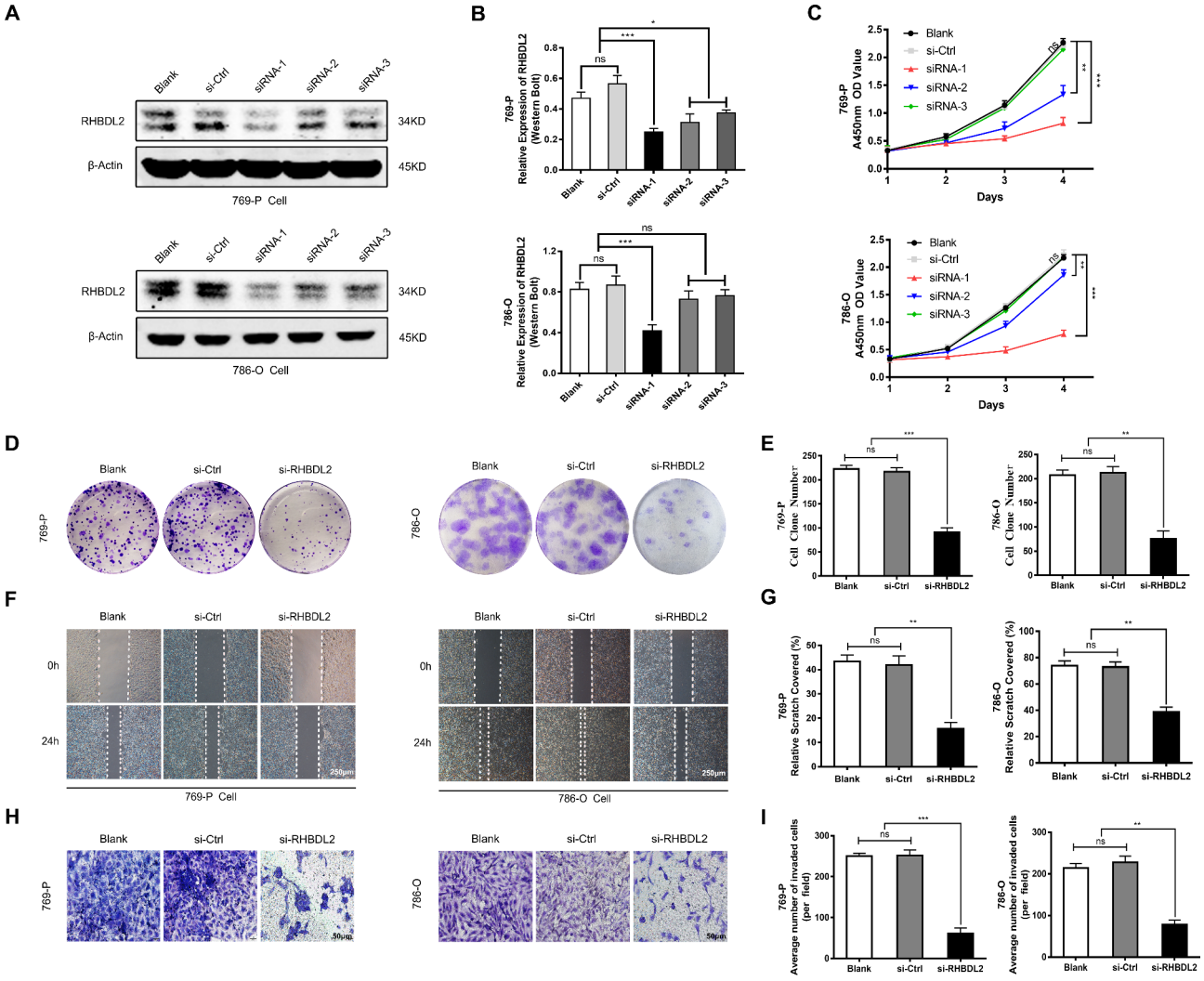

Fig. 6. Effects of *RHBDL2* knockdown on proliferation, migration, and invasion of the ccRCC cell lines 769-P and 786-O. (A, B) Western blots showing *RHBDL2* knockdown and siRNA-RHBDL2 sequence filtration in 769-P and 786-O cells (original blots are presented in Supplementary Fig. 5). (C) Effects of siRNA-1, siRNA-2, and siRNA-3 on 769-P and 786-O cell proliferation at 1, 2, 3, and 4 days detected using CCK-8 assays to confirm and select the optimal siRNA. (D) Colony formation assay results confirming that 769-P and 786-O cell growth rates exhibit a substantial reduction in the si-RHBDL2 group compared with that in the si-Ctrl and blank groups. (E) Quantitative analysis of colony formation assay results. (F, G) Wound healing assay demonstrating that *RHBDL2* knockdown suppresses 769-P and 786-O cells' migratory capacities (magnification: 40×, scale bar: 250 μm). (H, I) Transwell assay showing that *RHBDL2* knockdown reduces 769-P and 786-O cell invasion in the si-RHBDL2 group compared with that in the si-Ctrl group (magnification: 200×, scale bar: 50 μm). All experiments were performed in triplicate. $^{*}P < 0.05$, $^{**}P < 0.01$, $^{***}P < 0.001$; ns, nonsignificant.

siRNA-3 (all $P<0.01$; Fig. 6C). Collectively, these results revealed that siRNA-1 had the most efficient sequence for the knockdown of *RHBDL2* expression. Subsequent in vitro and in vivo experiments were thus executed using siRNA-1-transfected cells.

We conducted multiple in vitro experiments using *RHBDL2*-knockdown 769-P and 786-O cells to probe the effects of RHBDL2 on ccRCC cells' capacity to proliferate, migrate, and invade. By using colony formation assays, we evaluated the effects of *RHBDL2* knockdown on 769-P and 786-O cell proliferation. We noted considerable attenuation in cell proliferation in si-RHBDL2-treated 769-P and 786-O cells than in cells from the control and blank groups (all $P<0.01$; Fig. 6D and E). Similarly, our CCK-8 assay result demonstrated that the cell proliferation rate considerably decreased in the siRNA-1 group (Fig. 6C). Our wound healing assay for the influence of RHBDL2 on cell migration demonstrated more attenuation of migration in *RHBDL2*-knockdown cells than in the blank and si-Ctrl group cells (all $P<0.01$; Fig. 6F and G). The results of our transwell assay, evaluating invasion in response to *RHBDL2* knockdown in ccRCC cells, illustrated a significant reduction in the invasive capability of the si-RHBDL2 group cells compared with the blank and si-Ctrl group cells (all $P<0.01$; Fig. 6H and I). Therefore, RHBDL2 facilitates the proliferation, migration, and invasion of ccRCC cells in vitro, and it thus may be involved in the pathogenesis of ccRCC.

Regulation of CRGs and malignant phenotype by RHBDL2 via the Wnt/β-catenin pathway in ccRCC cells

The Wnt signaling pathway plays a crucial regulator of tissue cell homeostasis, cancer progression, cuproptosis activity, and TIME[13,26]. Next, we explored the intrinsic molecular modulatory mechanisms of RHBDL2, the Wnt/β-catenin pathway, and CRGs. We performed Western blotting in *RHBDL2*-knockdown 769-P and 786-O cells and detected the changes in CRGs and the vital Wnt/β-catenin pathway markers WNT3A and β-catenin[27]. We observed a substantial decrease in WNT3A and β-catenin expression in the RHBDL2-knockdown groups compared with that in the si-Ctrl groups. In contrast, *FDX1* and *LIAS* expression demonstrated a considerable increase in *RHBDL2*-knockdown cells (all $P<0.01$; Fig. 7A and B). We also treated *RHBDL2*-knockdown cells with HLY78, a specific agonist of the Wnt/β-catenin pathway[28], and our Western blotting results demonstrated that HLY78 treatment reduced FDX1 and LIAS expression decreased but increased WNT3A and β-catenin expression considerably (all $P<0.01$); in contrast, *RHBDL2* expression demonstrated no alterations (Fig. 7A and B). Furthermore, we assessed the effect of HLY78 on ccRCC cell proliferation and invasiveness through the CCK-8, colony formation, and transwell assays. The CCK-8 and colony formation assay results indicated that *RHBDL2*-knockdown cells treated with HLY78 regained their proliferative activity (all $P<0.01$; Fig. 7C and E). In addition, our transwell assay results demonstrated that HLY78 rescued the cell invasion ability of *RHBDL2*-knockdown cells (all $P<0.01$; Fig. 7F and G). Taken together, these results suggested that RHBDL2 suppresses *FDX1* and *LIAS* expression and promotes malignant progression of ccRCC through the Wnt/β-catenin pathway; these results are consistent with the results predicted by our bioinformatics analysis, verifying the accuracy of our predictions.

Validation of *RHBDL2* knockdown inducing CRG activity and reducing Treg-cell infiltration in vivo

We next explored the dynamic mechanisms between *RHBDL2* expression and TIME response and verified that RHBDL2 inhibits cuproptosis activity in ccRCC. We developed an in vivo subcutaneous tumor model by injecting *RHBDL2*-knockdown Renca cells into the right notum of BALB/c mice. By qRT-PCR, we verified a significant attenuation in RHBDL2 expression after transfection with si-RHBDL2 compared with that after transfection with blank or si-Ctrl in Renca cells (Supplementary Fig. 3). The mice tumor volumes and weights demonstrated a significant decrease in the si-RHBDL2 group compared with that in the si-Ctrl group ($P<0.01$; Fig. 8A and C). Subsequent HE staining demonstrated that the cell structure and morphology were disordered, and the nucleus was large and heterogeneous in the si-Ctrl group; however, after *RHBDL2*-knockdown, the tumor cell structure and morphology became regular (Fig. 8D). Our IHC results revealed that *RHBDL2*-knockdown increased FDX1 and LIAS expression but reduced that of FOXP3 (all $P<0.001$); for RHBDL2, FOXP3, FDX1, and LIAS, the expression levels were respectively 75.08 ± 9.60, 51.10 ± 8.52, 22.59 ± 6.03, and 28.03 ± 8.75 with si-Ctrl and 14.41 ± 7.97, 13.12 ± 5.59, 58.01 ± 9.66 and 64.23 ± 9.97 with si-RHBDL2 (Fig. 8D and E). After IF staining, Ki67 levels were measured to assess tumor cell proliferation ability; the results indicated that Ki67 levels were considerably lower in the si-RHBDL2 group than in the si-Ctrl group ($P<0.001$; Fig. 8F and G). Relative IF intensity of FOXP3 was detected to evaluate Treg-cell infiltration levels; the results demonstrated that FOXP3 expression was considerably attenuated after *RHBDL2*-knockdown ($P<0.01$; Fig. 8H and I). Taken together, these results demonstrated that RHBDL2 promotes renal tumor growth and inhibits CRG expression. The noted changes in FOXP3 expression suggested that RHBDL2 is involved in the regulation of Treg-cell infiltration; thus, RHBDL2 either modulates Treg-cell infiltration directly or via *RHBDL2*–CRG axes, leading to suppressive TIME formation. These findings are consistent with our bioinformatics predictions.

Discussion

Among all pathological subtypes of renal cancer, ccRCC demonstrates the highest incidence with the worst prognosis[4]. Recent studies have demonstrated that cuproptosis has a significant impact on tumor development and clinical immunotherapy[29]. However, the molecular mechanisms regulating the cross-talk between cuproptosis and the TIME, as well as their functions, in ccRCC have not been clarified. In this study, we, for the first time, identified *RHBDL2* as a crucial gene modulating the cuproptosis pathway based on clinical omics data of patients with ccRCC and well-designed bioinformatics pipelines. Here, through rigorous preclinical trials, we not only assessed how CRGs are regulated by RHBDL2 but also specifically investigated the influence of *RHBDL2* expression on ccRCC's malignant phenotype and TIME. We noted that RHBDL2 can mitigate cuproptosis

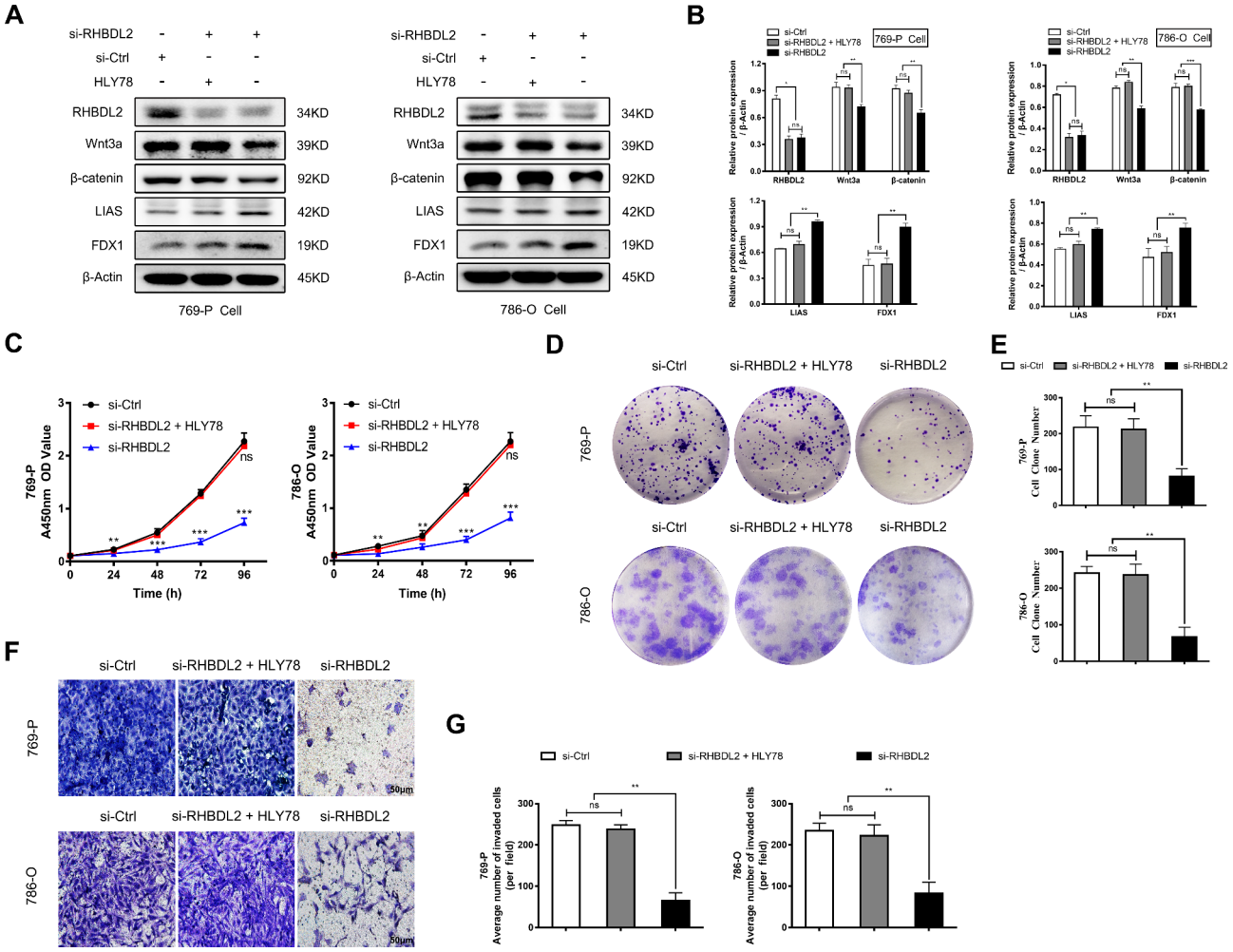

Fig. 7. RHBDL2 modulates the CRG pathways, as well as proliferation and invasion, through the Wnt/β-catenin pathway in ccRCC cells. (A) Western blot analysis showing that the protein expression levels of CRGs (FDX1 and LIAS) and Wnt/β-catenin pathway targets (WNT3A and β-catenin) in 769-P and 786-O cells are significantly rescued after HLY78 (10 μM) treatment for 48 h in the si-RHBDL2 group; however, RHBDL2 expression demonstrates no change (original blots are presented in Supplementary Fig. 6). (B) Relative quantitative measurements of various protein levels. (C–E) Proliferative capacities of *RHBDL2*-knockdown 769-P and 786-O cells pretreated with HLY78 (10 μM) for 48 h measured using CCK-8 (C) and colony formation (D, E) assays. (F) Transwell assay for cell invasiveness in si-RHBDL2 group cells pretreated with HLY78 (magnification: 200×, scale bar: 50 μm). (G) Quantitative analysis of transwell assay results. All experiments were performed in triplicate. $^{*}P<0.05$, $^{**}P<0.01$, $^{***}P<0.001$; ns, nonsignificant.

activity, promote malignant progression by modulating the typical carcinogenic Wnt/β-catenin pathway, and increase Treg-cell infiltration, resulting in a suppressive TIME in ccRCC, affording tumor cells with a survival advantage. Hence, oncologists consider that RHBDL2, with potential clinical translational value, might be a dual characteristic immune- and cuproptosis-related biomarker with utility in targeted therapy for ccRCC.

Recent studies have reported that RHBDL2 expression is considerably elevated in breast cancer tissues compared with the corresponding normal tissue and that it is closely associated with the pathological grade of breast cancer[30]. Battistini et al. reported that RHBDL2 promotes the migration and progression of prostate cancer cells through various experiments of RHBDL2 disturbed by shRNA in PC3 cells[31]. Consistent with previous results, we first used the Wilcoxon signed-rank test to assess TCGA data and found that RHBDL2 expression was high in the ccRCC tissues but low in the PC tissues; it was closely related to the survival and prognosis of clinical patients. Second, our in vitro *RHBDL2*-knockdown cell model demonstrated that depletion of RHBDL2 expression effectively reduced ccRCC cell proliferation, invasion, and migration. These findings were validated by the results in our preclinical mouse models, suggesting that *RHBDL2* knockdown considerably inhibits ccRCC tumor growth in vivo. Therefore, *RHBDL2* may be an oncogene, promoting the carcinogenesis and progression of ccRCC.

Many studies have shown that cuproptosis, copper-induced cell death, modulates tricarboxylic acid cycle metabolism to induce oxidative phosphorylation system dysfunction, leading to tumorigenesis[32]. In addition, FDX1 is a core molecule of cuproptosis occurrence; it reduces Cu^{2+} to the toxic Cu^{+}, which induces tumor

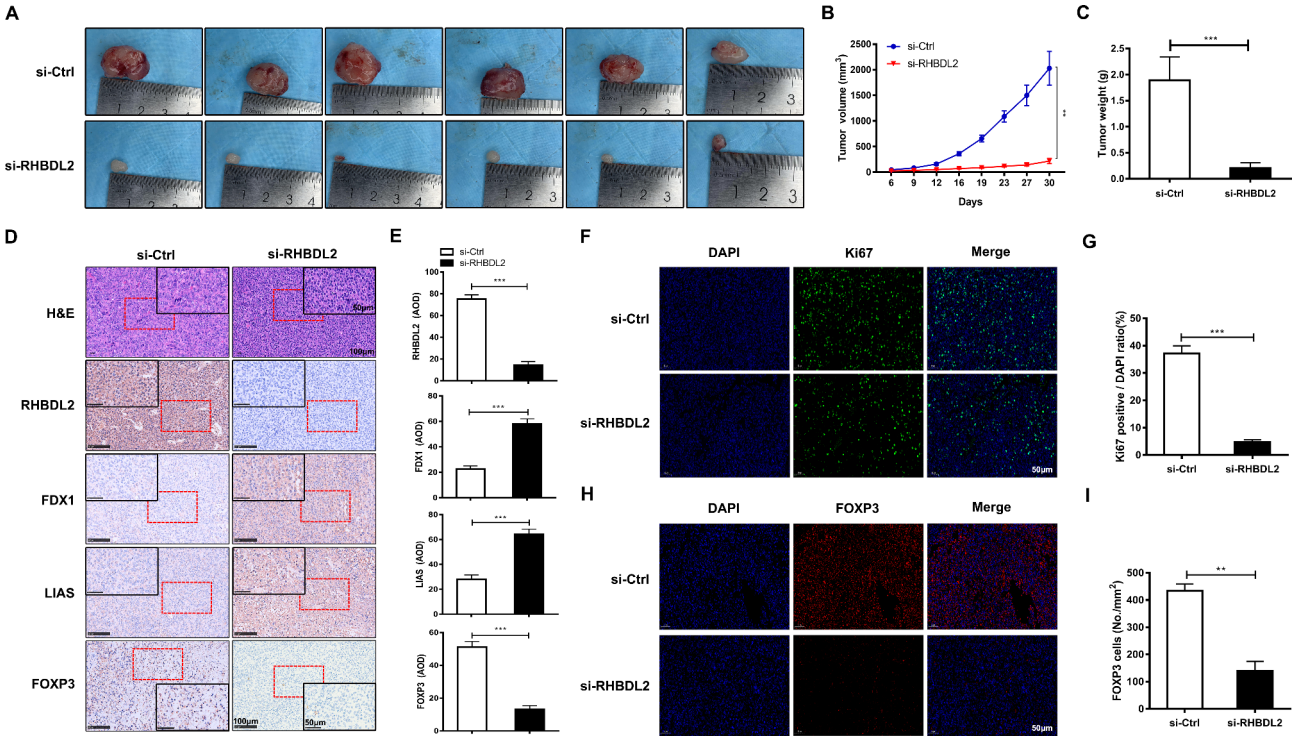

Fig. 8. *RHBDL2* knockdown suppresses tumor growth, activates CRG pathways, and reduces Treg-cell infiltration in vivo. (A) Representative images of BALB/c mouse with subcutaneous tumor models using Renca cells transfected with si-RHBDL2 or si-Ctrl. (B) Growth curves of subcutaneous tumor volume in the si-RHBDL2 and si-Ctrl groups mouse ($n = 8$). (C) Quantitative measurement and statistical analysis of subcutaneous tumor weight. (D, E) IHC for RHBDL2, FDX1, LIAS, and FOXP3 expression in our mouse tumor model. Renal tumor cell morphology observed using HE staining (magnifications: 100× and 200×, scale bars: 100 and 50 μm). (F, G) Effect of RHBDL2 on tumor cell proliferation in si-RHBDL2 and si-Ctrl group mice evaluated by measuring Ki67 expression (green) through IF (magnification: 200×, scale bar: 50 μm). (H) Fluorescence images of FOXP3 expression (red) for Treg-cell infiltration levels in our mouse tumor model after RHBDL2-knockdown (magnification: 200×, scale bar: 50 μm). (I) Semiquantitative measurement analysis of relative fluorescence intensity of FOXP3 to estimate Treg-cell infiltration levels. Representative experimental images are shown. All experiments were performed in triplicate. ** $P < 0.01$, *** $P < 0.001$.

cell death and modulates the lipoic acid pathway, thus mediating protein lipid acylation and thereby causing cuproptosis[33]. LIAS, an iron–sulfur cluster mitochondrial enzyme, is correlated with mitochondrial redox metabolism and participates in cuproptosis as a lipid acylation substrate of FDX1 [34]. Thus far, almost all relevant studies on cuproptosis in renal cancer have focused on the prognostic value and TME effects of the CRGs and RNA[35–37]. However, few studies have indicated the clinically feasible molecules that can induce cuproptosis in ccRCC. The results in our in vivo and in vitro models of *RHBDL2*-knockdown suggested that RHBDL2 acts as an upstream molecule that regulates *FDX1* and *LIAS* expression and thus mediates cuproptosis and promotes ccRCC progression. These results are consistent with the results predicted by our bioinformatics analysis model and fill the relevant cancer research gaps. Consequently, our findings shed new light on ccRCC therapy aimed at inducing cuproptosis and strongly promote the related research progress on cuproptosis in ccRCC.

As an independent prognosis predictor, cuproptosis-associated long noncoding RNA PCAT6 influences the Wnt pathway and regulates tumor development in hepatocellular carcinoma[38]. In the current study, the Spearman correlation coefficient demonstrated that the Wnt/β-catenin pathway was correlated with cuproptosis negatively and with *RHBDL2* expression positively in ccRCC. Subsequently, the Wnt pathway activator HLY78 was noted to reverse the trend of increases in FDX1 and LIAS expression and restored the levels of WNT3A and β-catenin, as well as the proliferation and invasion ability, in *RHBDL2*-knockdown 786-O and 769-P cells. However, the protein levels of RHBDL2 did not change. Thus, RHBDL2, the downstream regulator of the Wnt/β-catenin pathway, regulates CRGs and tumor metastasis through the Wnt/β-catenin pathway. In addition, low-density lipoprotein receptor-related protein 6 (LRP6) combined with frizzled receptors transmit the classical Wnt signal, and C1q bound to frizzled receptors causes the activation of C1s, a serine protease, which hydrolyzes LRP6 to trigger the canonical Wnt signaling pathway, leading to disease development[39]. Therefore, we speculate that RHBDL2, a serine proteolytic enzyme, may activate the Wnt pathway by cleaving the LRP6 receptor. Given the complexities of both RHBDL2 hydrolysis and the Wnt pathway, the specific molecular modulation mechanisms between RHBDL2 and the Wnt pathway warrant further exploration.

Some recent studies have indicated that the key CRG *PDHB*is negatively correlated with Treg cells and causes suppressive TIME formation primarily by controlling Treg-cell infiltration in renal cancer[25]. Similar results were found in the current study: RHBDL2 was positively correlated with Treg cells, macrophages, inflammation-promoting cells, parainflammatory cells, and cytolytic cells. This indicated that high RHBDL2 expression may facilitate suppressive TIME formation in ccRCC. In addition, Treg-cell dysfunction via various mechanisms aids tumor cells in escaping immune surveillance from the TME, thus weakening the body's anticancer response[40]. FOXP3, a member of the forkhead box family, is the pivotal transcriptional regulatory factor of Treg-cell development and function and regulates the Treg-cell–associated gene expression in cancer[41]. In this study, through machine learning, we found that Treg cells were correlated with *RHBDL2* expression positively but with cuproptosis and *FDX1* and *LIAS* expression negatively in ccRCC. Next, we preliminarily confirmed the aforementioned results through Western blotting, IHC, and IF staining of clinical tumor and PC tissue samples. Finally, through animal model experiments involving si-RHBDL2, we further confirmed that inhibiting *RHBDL2* expression reduced *FOXP3* expression and that *FOXP3* expression was negatively correlated with *FDX1* and *LIAS* expression. Thus, RHBDL2 may cause Treg-cell dysfunction, leading to the formation of a suppressive TIME and inducing tumor immune evasion in ccRCC. However, whether Treg cells are regulated by RHBDL2 directly or via the RHBDL2–FDX1–LIAS axis requires further investigation.

Conclusion

In summary, we, for the first time, identified *RHBDL2* as a novel oncogene, which induces cuproptosis via the Wnt/β-catenin pathway; moreover, it was noted to have dual characteristics in ccRCC: regulation of cuproptosis and immune infiltration. In particular, *RHBDL2* facilitates the malignant progression of ccRCC and inhibits CRGs via the Wnt/β-catenin pathway. It may reshape the TIME mainly through the modulation of Treg cells. Therefore, *RHBDL2* is a new potential ccRCC therapeutic target; it can be targeted to regulate both cuproptosis and immunity in patients with ccRCC.

Materials and methods

Data collection and treating

We collected the RNA-seq and clinical data of 607 patients diagnosed as having ccRCC from TCGA (www.tcga.org) database. However, patients with missing or incomplete information (survival or event) were excluded. Finally, a total of 527 patients with ccRCC were included in subsequent analyses. We also searched the Genotype-Tissue Expression Project (www.genome.gov) data for RNA-seq data from 84 healthy kidney tissues. All RNA-seq data were obtained as raw counts, which were converted to normalized counts. The data were integrated, and the batch effect was removed using the R package ComBat. Next, we used the R package DeMixT to deconvolute the RNA-seq data and extract the expression data of purified tumor cells. Then, these data were TPM-converted using the human reference genome (GRCh38–hg38) for further data normalization. Finally, the TPM values were converted for further analysis as follows:

$$Gene\ expression = log_2(TPM + 1)$$

The data included in this study were obtained between October 3 and 27, 2020.

Tailored machine learning for screening key genes associated with cuproptosis regulation and ccRCC progression

We established a tailored machine learning pipeline to identify genes associated with cuproptosis and ccRCC progression. It was a two-step program.

Step 1 included cuproptosis scoring and clinical implications analysis. Based on the processed RNA-seq data, the cuproptosis activity in normal and ccRCC tissues was determined. The CRG set was obtained from a previous study[22]. We used the R package Singscore, widely used for scoring gene sets in single-cell data, to determine differentially expressed gene (DEG) sets in all samples. Singscore is a rank-based single-sample scoring technique designed for stable, interpretable molecular phenotyping. It ranks genes based on transcript abundance, normalizes mean ranks, and sums them to provide a score ranging from − 1 to 1. This score indicates the concordance of a sample's transcriptome with a specified signature, reflecting the relative mean percentile rank of target gene sets within each sample. Singscore is particularly effective in terms of its simplicity, speed, and stability, making it highly suitable for clinical and research applications. The difference in cuproptosis activity between normal and ccRCC tissues was determined using the Wilcoxon signed-rank test. We also employed the Wilcoxon signed-rank test to ascertain the effects of the key genes associated with cuproptosis regulation and those of cuproptosis on ccRCC progression based on the pathology grade and TNM classification.

Step 2 involved screening key genes associated with cuproptosis regulation and ccRCC progression. The key genes involved in cuproptosis were identified using a screening process based on earlier work[23] but with a minor modification. In brief, Kaplan–Meier (KM) survival curves and univariate Cox regression analysis were used to discover genes strongly associated with ccRCC prognosis. Only genes with $P < 0.001$ in both the KM survival curve and univariate analyses were retained. By using the Spearman correlation coefficient, a tool for assessing the degree of correlation between skewed variables, we investigated the gene–cuproptosis activity relationships.

ESTIMATE, ssGSEA, and CIBERSORT for TIME analysis

Based on a previous study[23], we measured the immune, stromal, and ESTIMATE scores as well as the tumor purity of ccRCC samples by employing the estimation of stromal and immune cells in malignant tumor tissues using expression data (ESTIMATE) algorithm. We conducted the Wilcoxon signed-rank test to analyze the data and evaluate whether a substantial difference existed in the TME across the two groups. Subsequently, we

assessed the infiltration levels of 29 distinct immune cell types present in ccRCC by using single-sample gene sets enrichment analysis (ssGSEA) and cell type identification by estimating relative subsets of RNA transcripts (CIBERSORT). We employed the Wilcoxon signed-rank test to establish whether there was a substantial variation in terms of the infiltration levels of immune cells in tumors across groups. Furthermore, the Spearman correlation coefficient was used to determine the correlation among data.

Human tissue samples

We obtained the ccRCC tissues of 12 patients from the Department of Urology at Renmin Hospital of Wuhan University (approval no. 2017 K-C015) from May 19 2017 to May 19 2018. The ccRCC and corresponding non-ccRCC tissues were diagnosed and validated by an experienced pathologist. To conduct immunohistochemistry (IHC) and immunofluorescence (IF) analyses, each tissue sample was fixed in 4% paraformaldehyde. During every stage of our experiments, we adhered to the guidelines outlined in the Code of Ethics of the World Medical Association.

The Ethics Committee of Renmin Hospital of Wuhan University conducted a review of our research and granted approval. All methods were performed in accordance with the relevant guidelines and regulations. After receiving sufficient information, all participants enrolled in this study provided their written consent.

Cell culture and treatment

We obtained representative human ccRCC cell lines 786-O and 769-P from ASY Biotechnology Ltd., Corp (Wuhan, China). All cells were cultured in 89% Roswell Park Memorial Institute 1640 medium (Life Technologies, Gibco, USA) supplemented with 10% fetal bovine serum (Life Technologies) and 1% penicillin–streptomycin (Life Technologies) unless stated otherwise. The cells were incubated in a culture flask at 37 °C in a humidified incubator with 5% CO_2 until they reached 85–95% confluency. They were then trypsinized and harvested for subsequent experiments.

Small interfering RNA construction and transfection

Three *RHBDL2*-specific small interfering RNAs (siRNAs) were used to knock down *RHBDL2* (si-RHBDL2) expression. The following three siRNAs and negative control siRNA (si-Ctrl) were procured from Sangon Biotech (Shanghai, China):

- si-Ctrl: 5′- UUCUCCGAACGUGUCACGUTT-3′.
- siRNA-1: 5′-CUGGCAGUGUUUAUUUACUAUTT-3′.
- siRNA-2: 5′-CCCUUGGAAAUGGUCCACAAATT −3′.
- siRNA-3: 5′-GCAUAUUUAGCUUGUGUCUUATT-3′.
- si-Ctrl-mouse: 5′-CCUUGACUCGUUGGUGAGUCCAUCATT-3′.
- si-RHBDL2-mouse: 5′-CCUCAAGUCUCUUGUGGGAGCUUCATT-3′.

Before transfection, the cells were cultured until 60–70% confluency, and the medium was replaced with a serum- and antibiotic-free medium. To transfect the cells with siRNA, we used Lipofectamine 2000 (#11668019; Invitrogen, Thermo Fisher Scientific, Waltham, MA, USA), according to the manufacturer's instructions. After 48 h of transfection, we determined the transfection efficacy using Western blotting.

qRT-PCR

The RHBDL2 expression level was measured by qRT-PCR. Briefly, the collected samples were homogenized, and the total RNA was extracted via TRIZOL method. Afterwards, the cDNA was transcribed according to the instruction of kit provider (Takara, Japan). Once the cDNA was transcribed, we further using qPCR mix kit (Takara, Japan) to detect the relative expression of targeted gene. The primers used in the present study were: RHBDL2 forward: 5′-ATGGCTGTTGCTCACGAGATG-3′, reverse: 5′-GCTCCTGGGGAAGTCTTTACC-3′; and β-actin forward: 5′-GGCTGTATTCCCCTCCATCG-3′, reverse: 5′-CCAGTTGGTAACAATGCCATGT-3′.

Western blotting

The cells were lysed using RIPA buffer (Beyotime Biotechnology, Shanghai, China), protease inhibitor cocktail (Roche, Basel, Switzerland), and phenylmethylsulfonyl fluoride (Beyotime Biotechnology) in a volume ratio of 100:4:1 for 30 min on ice. A bicinchoninic acid protein assay kit (Beyotime Biotechnology) was used to measure the protein concentration accurately. A 5× sodium dodecyl sulfate-polyacrylamide gel electrophoresis (SDS-PAGE) sample loading buffer (Beyotime Biotechnology) was employed for mixing the protein samples. In addition, 30 μg of the proteins were isolated on 15% SDS-PAGE gel (Biotechwell, Shanghai, China) and transferred onto polyvinylidene difluoride (PVDF) membranes (#IPFL00010; Millipore, USA). Thereafter, the PVDF membranes were blocked with 5% skimmed milk (#232100; BD Biosciences, USA) for 2 h, followed by incubation with primary antibodies at 4 °C overnight. Next, the samples were incubated with fluorescence-labeled secondary antibodies for 2.5 h in the dark. The Odyssey infrared imaging equipment (LI-COR Biosciences, USA) was used to scan and develop the membranes (The reason for cutting blots was that these original informations could evidence our data). The grayscale value of the experiment was analyzed using ImageJ. The primary antibodies used for Western blotting were anti-RHBDL2 (#PA5-112693; Thermo Fisher Scientific), anti-RHBDL2 (#12467-1-AP; Proteintech, USA), anti-WNT3A (#ab81614; Abcam, UK), anti-β-catenin (#8480S; Cell Signaling Technology, USA), anti-LIAS (#11577-1-AP; Proteintech, USA), anti-FDX1 (#12592-1-AP; Proteintech), anti-FOXP3 (#22228-1-AP; Proteintech), anti-β-actin (#3700S; Cell Signaling Technology). Fluorescence-labeled secondary antibodies goat antimouse (#926-32210; LI-COR Bioscience) and goat antirabbit (#926-32211; LI-COR Bioscience) with IRDye 800CW were used.

IHC and hematoxylin–eosin staining

The tissue samples obtained from patients with ccRCC were embedded in paraffin after treatment with 4% paraformaldehyde. The paraffin-embedded tissues were sectioned, dewaxed using xylene for 20 min, rehydrated using ethanol for 30 min, and stained with hematoxylin and eosin (HE).

For IHC, dewaxed and rehydrated sections were exposed to a sodium citrate buffer (pH = 6.0) to retrieve the antigens. After they were blocked with 5% goat serum for 40 min, the sections were incubated with primary antibodies against RHBDL2 (1:50; #PA5-112693; Thermo Fisher Scientific), FDX1 (1:100; #12592-1-AP; Proteintech), LIAS (1:100, #11577-1-AP; Proteintech), and FOXP3 (1:200, #12653T; CST) at 4 °C overnight. Then, the sections were exposed to a horseradish peroxidase–labeled secondary antibody (Beyotime Biotechnology) at room temperature for 1 h. The sections were counterstained with hematoxylin. The tissues were imaged under an orthophoto microscope (BX63; Olympus, Japan).

IF staining

The tissue samples obtained from patients with ccRCC were embedded in paraffin after treatment with 4% paraformaldehyde. The paraffin-embedded sections were dewaxed using xylene, then rehydrated using ethanol, and finally blocked using 5% bovine serum albumin. The sections were then exposed to primary antibodies against RHBDL2 (1:100; Thermo Fisher Scientific), FDX1 (1:200; Proteintech), Ki67 (1:200, #ab16667; Abcam), and FOXP3 (1:500, #12653T; CST). We used 4′,6-diamidino-2-phenylindole (DAPI) for nucleus staining. We used fluorescence microscopy on an Olympus BX63 to capture images of the sections.

Cell counting Kit-8 and colony formation assays

Cell proliferation was assessed using the Cell Counting Kit-8 (CCK-8; #CK04; Dojindo, Japan), according to the manufacturer's instructions. To ascertain the impact of RHBDL2 on ccRCC cell proliferation, 769-P or 786-O cells transfected with si-Ctrl or si-RHBDL2 were seeded at 3,000 cells/well in a 96-well plate and cultured in 150 μL of fresh complete medium. After incubation of the cells with CCK-8 reagents for 1 h, absorbance was measured at 450 nm on a multiwell plate detector (Perkin Elmer, Singapore) at 1, 2, 3, and 4 days.

A colony formation assay was performed to examine the effects of *RHBDL2* knockdown on the growth potential of ccRCC cells. In brief, 769-P or 786-O cells transfected with the si-Ctrl or si-RHBDL2 were seeded at 600 cells/well in six-well plates and assessed after 15 days. The formed cell colonies were enumerated using Image J. Each experiment was performed in triplicate, and the data are presented as means ± standard deviations (SDs).

Wound healing assay

We cultured 786-O and 769-P cells until they reached 85–90% confluency in six-well plates. A scratch was made using a sterile 1-mL plastic tip. Microscopic images were captured at 0 and 24 h to assess wound healing. The following equation was used for calculating wound healing percentage:

Wound healing percentage = [(0-h scratch area – 24-h scratch area)/0-h scratch area] × 100%.

By measuring the healed wound area, we assessed the effects of *RHBDL2* knockdown on the migratory capacities of ccRCC cells. This experiment was performed in triplicates.

Cell invasion assay

We performed an invasion assay in 24-well transwell plates (#3422; Corning, USA). Matrigel matrix (#356234; BD Biosciences, USA) was diluted in a basal medium at a 1:8 ratio to cover the bottom well. Next, 2×10^5 cells suspended in 100 μL of basal medium were seeded in the transwell plate for 48 h, allowing for the cells to invade through the bottom well. After fixing the transwells with 75% ethanol for 30 min, we dyed the cells with 0.05% crystal violet for 1 h. Images were captured under a microscope. To measure the invasive capability of cells, we enumerated cells invading the Matrigel using ImageJ.

In vivo subcutaneous tumor model

Murine renal cancer cell line Renca from ASY Biotechnology Ltd., Corp (transfected with si-RHBDL2 or si-Ctrl) was resuspended at a concentration of 2×10^5 cells/μL in 100 μL of phosphate-buffered saline with 50% Matrigel. Female wildtype BALB/c mice ($n = 16$) aged 6 weeks received the cells through subcutaneous injection into their right notum. Vernier calipers were used to measure the diameter of the subcutaneous tumor in mice at 3-day intervals. The following equation was used to determine the tumor volume:

Tumor volume (mm^3) = 0.5 × Tumor length (mm) × Tumor width^2(mm^2).

After 30 days, all mice were euthanized by CO2 inhalation overdose transiently; their subcutaneous tumors were extracted, weighed, and preserved. The paraffin-embedded sections were used to perform HE, IHC, and IF staining to determine the effects of RHBDL2 on cuproptosis and Treg-cell infiltration. All experiments involving animals were executed in conformity to ARRIVE guidelines and the National Institutes of Health Guide for the Care and Use of Laboratory animals and approved by the Medical Ethical Committee of Renmin Hospital of Wuhan University.

Statistical analysis

The Wilcoxon signed-rank test was applied to analyze clinical characteristics and factors. KM survival analysis was used to analyze the differences in survival between the high- and low-expression patient groups. Univariate Cox regression analysis was used to discover DEGs. All experiments were performed with at least three independent biological replicates. All data are expressed as means ± standard deviation (SDs).

We employed R (version 4.3.1), SPSS (version 25.0; IBM, USA), and GraphPad Prism (version 7; GraphPad Software, USA) for all statistical analyses. The data obtained from clinical tissues and from in vitro and in vivo

experiments were examined using the Student's *t*-test or one-way analysis of variance. The criterion for statistical significance was set at $P < 0.05$.

Data availability

All data generated or analyzed during this study are available from the corresponding author upon reasonable request.

Received: 17 February 2024; Accepted: 4 November 2024
Published online: 07 November 2024

References

1. Weaver, C. et al. Diagnostic and prognostic biomarkers in Renal Clear Cell Carcinoma. *Biomedicines*. **10** https://doi.org/10.3390/biomedicines10112953 (2022).
2. Che, Z. et al. Activation-Induced Cytidine Deaminase expression facilitates the malignant phenotype and epithelial-to-mesenchymal transition in Clear Cell Renal Cell Carcinoma. *DNA Cell. Biol.* **39**, 1299–1312. https://doi.org/10.1089/dna.2019.5119 (2020).
3. Siegel, R. L., Miller, K. D., Fuchs, H. E. & Jemal, A. Cancer statistics, 2022. *CA Cancer J. Clin.* **72**, 7–33. https://doi.org/10.3322/caac.21708 (2022).
4. Ljungberg, B. et al. European Association of Urology Guidelines on Renal Cell Carcinoma: the 2022 Update. *Eur. Urol.* **82**, 399–410. https://doi.org/10.1016/j.eururo.2022.03.006 (2022).
5. Barata, P. C. & Rini, B. I. Treatment of renal cell carcinoma: current status and future directions. *CA Cancer J. Clin.* **67**, 507–524. https://doi.org/10.3322/caac.21411 (2017).
6. Peng, X. et al. Signature construction and molecular subtype identification based on cuproptosis-related genes to predict the prognosis and immune activity of patients with hepatocellular carcinoma. *Front. Immunol.* **13**, 990790. https://doi.org/10.3389/fimmu.2022.990790 (2022).
7. Zhao, Q. & Qi, T. The implications and prospect of cuproptosis-related genes and copper transporters in cancer progression. *Front. Oncol.* **13**, 1117164. https://doi.org/10.3389/fonc.2023.1117164 (2023).
8. Zhang, G., Sun, J. & Zhang, X. A novel cuproptosis-related LncRNA signature to predict prognosis in hepatocellular carcinoma. *Sci. Rep.* **12**, 11325. https://doi.org/10.1038/s41598-022-15251-1 (2022).
9. Sha, S. et al. Prognostic analysis of cuproptosis-related gene in triple-negative breast cancer. *Front. Immunol.* **13**, 922780. https://doi.org/10.3389/fimmu.2022.922780 (2022).
10. Li, Y. Copper homeostasis: emerging target for cancer treatment. *IUBMB Life*. **72**, 1900–1908. https://doi.org/10.1002/iub.2341 (2020).
11. Bian, Z., Fan, R. & Xie, L. A. Novel cuproptosis-related prognostic gene signature and validation of Differential expression in Clear Cell Renal Cell Carcinoma. *Genes (Basel)*. 13. https://doi.org/10.3390/genes13050851 (2022).
12. Liu, X., Luo, B., Wu, X. & Tang, Z. Cuproptosis and cuproptosis-related genes: emerging potential therapeutic targets in breast cancer. *Biochim. Biophys. Acta Rev. Cancer*. **1878**, 189013. https://doi.org/10.1016/j.bbcan.2023.189013 (2023).
13. Cong, T. et al. Cuproptosis-related immune checkpoint gene signature: prediction of prognosis and immune response for hepatocellular carcinoma. *Front. Genet.* **13**, 1000997. https://doi.org/10.3389/fgene.2022.1000997 (2022).
14. Etheridge, S. L., Brooke, M. A., Kelsell, D. P. & Blaydon, D. C. Rhomboid proteins: a role in keratinocyte proliferation and cancer. *Cell. Tissue Res.* **351**, 301–307. https://doi.org/10.1007/s00441-012-1542-1 (2013).
15. Fleig, L. et al. Ubiquitin-dependent intramembrane rhomboid protease promotes ERAD of membrane proteins. *Mol. Cell.* **47**, 558–569. https://doi.org/10.1016/j.molcel.2012.06.008 (2012).
16. Lemberg, M. K. & Freeman, M. Functional and evolutionary implications of enhanced genomic analysis of rhomboid intramembrane proteases. *Genome Res.* **17**, 1634–1646. https://doi.org/10.1101/gr.6425307 (2007).
17. Chen, S. et al. RHBDL2 promotes the proliferation, migration, and invasion of pancreatic cancer by stabilizing the N1ICD via the OTUD7B and activating the notch signaling pathway. *Cell. Death Dis.* **13**, 945. https://doi.org/10.1038/s41419-022-05379-3 (2022).
18. Ishii, S., Merlino, G. T. & Pastan, I. Promoter region of the human Harvey Ras proto-oncogene: similarity to the EGF receptor proto-oncogene promoter. *Science*. **230**, 1378–1381. https://doi.org/10.1126/science.2999983 (1985).
19. Uyttendaele, H. et al. Notch4/int-3, a mammary proto-oncogene, is an endothelial cell-specific mammalian notch gene. *Development*. **122**, 2251–2259. https://doi.org/10.1242/dev.122.7.2251 (1996).
20. Chevrier, S. et al. An Immune Atlas of Clear Cell Renal Cell Carcinoma. *Cell* 169, 736–749 e718, doi: (2017). https://doi.org/10.1016/j.cell.2017.04.016
21. Zhang, Z. et al. Cuproptosis-related risk score predicts prognosis and characterizes the Tumor Microenvironment in Hepatocellular Carcinoma. *Front. Immunol.* **13**, 925618. https://doi.org/10.3389/fimmu.2022.925618 (2022).
22. Tsvetkov, P. et al. Copper induces cell death by targeting lipoylated TCA cycle proteins. *Science*. **375**, 1254–1261. https://doi.org/10.1126/science.abf0529 (2022).
23. Jin, W. et al. Exploration of the molecular characteristics of the tumor-immune interaction and the development of an individualized immune prognostic signature for neuroblastoma. *J. Cell. Physiol.* **236**, 294–308. https://doi.org/10.1002/jcp.29842 (2021).
24. Morina, L. et al. Co-expression of Foxp3 and Helios facilitates the identification of human T regulatory cells in health and disease. *Front. Immunol.* **14**, 1114780. https://doi.org/10.3389/fimmu.2023.1114780 (2023).
25. Wu, J. et al. Integrated single-cell and bulk characterization of cuproptosis key regulator PDHB and association with tumor microenvironment infiltration in clear cell renal cell carcinoma. *Front. Immunol.* **14**, 1132661. https://doi.org/10.3389/fimmu.2023.1132661 (2023).
26. Parsons, M. J., Tammela, T. & Dow, L. E. WNT as a driver and dependency in Cancer. *Cancer Discov.* **11**, 2413–2429. https://doi.org/10.1158/2159-8290.CD-21-0190 (2021).
27. Abu-Elfotuh, K. et al. The protective effects of sesamol and/or the probiotic, Lactobacillus rhamnosus, against aluminum chloride-induced neurotoxicity and hepatotoxicity in rats: modulation of Wnt/beta-catenin/GSK-3beta, JAK-2/STAT-3, PPAR-gamma, inflammatory, and apoptotic pathways. *Front. Pharmacol.* **14**, 1208252. https://doi.org/10.3389/fphar.2023.1208252 (2023).
28. Si, J. et al. Effects of ionizing radiation and HLY78 on the zebrafish embryonic developmental toxicity. *Toxicology*. **411**, 143–153. https://doi.org/10.1016/j.tox.2018.10.004 (2019).
29. Ran, X. M. et al. The effect of cuproptosis-relevant genes on the immune infiltration and metabolism of gynecological oncology by multiply analysis and experiments validation. *Sci. Rep.* **13**, 19474. https://doi.org/10.1038/s41598-023-45076-5 (2023).
30. Canzoneri, R., Lacunza, E., Isla Larrain, M., Croce, M. V. & Abba, M. C. Rhomboid family gene expression profiling in breast normal tissue and tumor samples. *Tumour Biol.* **35**, 1451–1458. https://doi.org/10.1007/s13277-013-1199-8 (2014).
31. Battistini, C. et al. Rhomboid-Like-2 intramembrane protease mediates metalloprotease-independent regulation of cadherins. *Int. J. Mol. Sci.* **20** https://doi.org/10.3390/ijms20235958 (2019).

32. Long, S. et al. Pan-cancer analysis of cuproptosis regulation patterns and identification of mTOR-target responder in clear cell renal cell carcinoma. *Biol. Direct*. **17**, 28. https://doi.org/10.1186/s13062-022-00340-y (2022).
33. Quan, Y. et al. Tumor cuproptosis and immune infiltration improve survival of patients with hepatocellular carcinoma with a high expression of ferredoxin 1. *Front. Oncol.* **13**, 1168769. https://doi.org/10.3389/fonc.2023.1168769 (2023).
34. Li, Y. et al. Exploring the role of LIAS-related cuproptosis in systemic lupus erythematosus. *Lupus*. **9612033231211429** https://doi.org/10.1177/09612033231211429 (2023).
35. Mei, W. et al. A cuproptosis-related Gene Model for Predicting the prognosis of Clear Cell Renal Cell Carcinoma. *Front. Genet.* **13**, 905518. https://doi.org/10.3389/fgene.2022.905518 (2022).
36. Xie, M. et al. Cuproptosis-related MiR-21-5p/FDX1 Axis in Clear Cell Renal Cell Carcinoma and its potential impact on Tumor Microenvironment. *Cells*. **12** https://doi.org/10.3390/cells12010173 (2022).
37. Huili, Y. et al. Cuproptosis-related lncRNA: prediction of prognosis and subtype determination in clear cell renal cell carcinoma. *Front. Genet.* **13**, 958547. https://doi.org/10.3389/fgene.2022.958547 (2022).
38. Yang, L. et al. Creation of a Prognostic Model using cuproptosis-Associated Long Noncoding RNAs in Hepatocellular Carcinoma. *Int. J. Mol. Sci.* **24** https://doi.org/10.3390/ijms24129987 (2023).
39. Lu, J. & Kishore, U. C1 complex: an adaptable Proteolytic Module for complement and non-complement functions. *Front. Immunol.* **8**, 592. https://doi.org/10.3389/fimmu.2017.00592 (2017).
40. Liu, Z. et al. Why Treg should be the focus of cancer immunotherapy: the latest thought. *Biomed. Pharmacother*. **168**, 115142. https://doi.org/10.1016/j.biopha.2023.115142 (2023).
41. Dong, Y., Yang, C. & Pan, F. Post-translational regulations of Foxp3 in Treg Cells and their therapeutic applications. *Front. Immunol.* **12**, 626172. https://doi.org/10.3389/fimmu.2021.626172 (2021).

Acknowledgements

The authors would like to thank their colleagues at the Central Laboratory of Renmin Hospital, Wuhan University, where most of this work was performed.

Author contributions

Peiyu Liang, Haoyong Li, and Zhifei Che contributed to the conceptualization and design of the study; Peiyu Liang and Zhifei Che: funding acquisition; Zhifei Che and Peiyu Liang: writing the initial draft of the manuscript; Peiyu Liang and Haoyong Li: reviewing and editing the manuscript; Zhifei Che and Wenyi Jin: bioinformatics analysis; Zhifei Che and Yaoxi Wu: performed in vitro and in vivo experiments; Zhifei Che, Yaoxi Wu and Wenyi Jin: conducted data analysis. All authors reviewed the manuscript.

Funding

This study was supported by the Special fund project for Science and Technology of Social Development of Hainan Province (Grant No. ZDYF2020136) and the Graduate Innovation Research Project of Hainan Province (Grant No. Qhyb2021-57).

Declarations

Ethics approval and consent to participate

The study of human tissue samples was approved by the Ethics Committee of Renmin Hospital of Wuhan University. Informed consent was obtained from all participants. All experiments involving animals were executed in conformity to ARRIVE guidelines and the National Institutes of Health Guide for the Care and Use of Laboratory animals and approved by the Medical Ethical Committee of Renmin Hospital of Wuhan University.

Competing interests

The authors declare no competing interests.

Additional information

Supplementary Information The online version contains supplementary material available at https://doi.org/10.1038/s41598-024-78713-8.

Correspondence and requests for materials should be addressed to H.L. or P.L.